Limit analysis as a tool for the simplified assessment of ancient masonry structures

Agustín Orduña and Paulo B. Lourenço
University of Minho, Department of Civil Engineering, Guimarães, Portugal

ABSTRACT: This paper presents a general method for the limit analysis of structures made of rigid blocks, which can be used in the assessment of ancient masonry structures. This method takes into account non-associated flow rules and a limited compressive stress for the masonry. Some results, obtained by a computer implementation of the method, are presented and discussed.

1 INTRODUCTION

The engineering assessment of ancient masonry structures requires practical computational tools. Non-linear finite element approaches are a possible choice for masonry structures assessment. Both advanced continuous, anisotropic based models, and discrete (micro-) models for masonry structures have been developed in the last decades, e.g. Lourenço and Rots (1997) and Lourenço et al. (1998). Nevertheless, the drawback of using non-linear finite element analysis in practice might include: (a) requirement of adequate knowledge of sophisticated non-linear processes and advanced solution techniques by the practitioner; (b) comprehensive mechanical characterization of the materials; and (c) large time requirements for modelling, for performing the analyses themselves, with a significant number of load combinations, and for reaching proper understanding of the results significance. Of course, for special cases, as complex, important or large structures, non-linear analysis should not be disregarded as an analysis tool.

Linear-elastic analysis can be assumed more practical, even if the time requirements of modelling are similar. Nevertheless, such an analysis fails to give an idea of the structural behaviour beyond the beginning of cracking. Due to the low tensile strength of masonry, linear elastic analyses seem to be unable to represent adequately the behaviour of historical constructions.

Limit analysis combines, on one side, sufficient insight into collapse mechanisms, ultimate stress distributions (at least on critical sections) and load capacities, and, on the other, simplicity to be cast in a practical computational tool. Another appealing feature of limit analysis is the reduced number of necessary material parameters, given the difficulties in obtaining reliable data for historical masonry.

Livesley (1978), was the first author to apply the limit analysis theory to rigid block arches, by means of the static theorem. More recently, Gilbert and Melbourne (1994) applied the kinematics theorem to the same problem, aiming at analysing masonry arch bridges. Begg and Fishwick (1995) have released the restriction of associated flow rule or normality condition for masonry arches, including sliding shear failure. This aspect was also addressed by Baggio and Trovalusci (1998) in a general formulation for rigid block limit analysis. It is noted that extending the formulation to non-associated flow, results in a non-linear mathematical problem of a significantly larger size, in comparison with the lower size linear problem resulting from the classical theory.

In the following, a limit analysis formulation for two-dimensional structures made from rigid blocks is presented. This formulation accounts for a limited compressive stress in the masonry, and non-associated flow rules for sliding failure. Some computational techniques developed to

improve the solution of the resulting non-linear mathematical problem are also presented. The model is implemented in a computer program, with the purpose of developing a suitable tool for engineering practice analysis of masonry structures. Aiming at evaluating the proposed formulation performance, the numerical results of some arches and shear walls models are compared with experimentally obtained results.

2 LIMIT ANALYSIS FORMULATION

The approach presented here assumes that the small displacements hypothesis is valid. It is also assumed that masonry structures are made from perfectly rigid blocks. Finally, the interface between two blocks cannot withstand tensile stresses, can withstand limited compressive stresses, and the shear failure is controlled by the Coulomb's law.

The static variables, or generalized stresses, at an interface k are selected to be the shear force, V_k, the normal force, N_k, and the moment, M_k, all at the centre of the joint. Correspondingly, the kinematic variables, or generalized strains, are the relative tangential, normal and angular displacement rates, dn_k, ds_k and $d?_k$ at the interface centre, respectively. The degrees of freedom are the displacement rates in the x and y directions, and the angular change rate of the centroid of each block: du_i, dv_i and df_i for the block i. In the same way, the external loads are described by the forces in x and y directions, as well as the moment at the centroid of the block. The loads are split in a constant part (with a subscript c) and a variable part (with a subscript v): f_{cxi}, f_{vxi}, for the forces in the x direction, f_{cyi}, f_{vyi}, for the forces in the y direction, and m_{ci}, m_{vi}, for the moments. These variables are arranged in the vectors of generalized stresses $\mathbf{Q}$, generalized strains $d\mathbf{q}$, displacements rates $d\mathbf{u}$, constant loads $\mathbf{F_c}$, and variable loads $\mathbf{F_v}$. Finally, the load factor a is defined, measuring the amount of the variable load vector applied to the structure, and whose limit value is looked for. In this way, the total load vector $\mathbf{F}$ is given by Eq. (1).

$$\mathbf{F} = \mathbf{F_c} + a\mathbf{F_v} \tag{1}$$

2.1 Yield function

The yield function at each joint is composed by the crushing-hinging criterion and the Coulomb criterion. For the crushing-hinging criterion, it is assumed that the normal force is equilibrated by a constant stress distribution near the edge of the joint, see Fig. 1a. The stress value is f_{cef}, given by Eq. (2), borrowed from the concrete plasticity theory (Nielsen, 1998). Here, f_c is the compressive strength of the material, and $?$ is an effectiveness factor, which takes into account reductions in the compressive strength due to transverse cracking, as well as the fact that limit analysis assumes a rigid-plastic behaviour, while, in fact, significant softening occurs. Eq. (3) is an expression for the effectiveness factor commonly used for concrete (Nielsen, 1998), where f_c is the measured compressive strength expressed in N/mm^2.

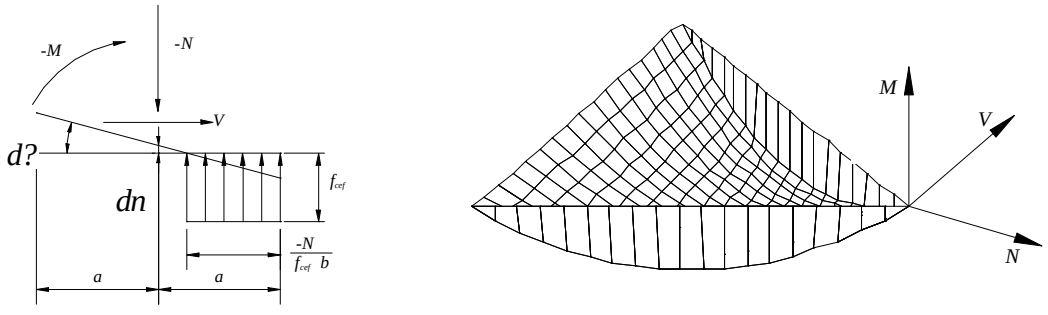

(a) (b)

Figure 1: (a) Joint generalized stresses and strains for the crushing-hinging failure mode; (b) geometric representation of a half of the yield surface.

$$f_{cef} = nf_c \tag{2}$$

$$n = 0.7 - \frac{f_c}{200} \tag{3}$$

The constant stress distribution hypothesis leads to the yield function given by Eq. (4); note that N_k represents a non-positive value. The Coulomb criterion is expressed by Eq. (5). It is stressed that the complete yield function is composed by four surfaces, two given by Eq. (4) and two given by Eq. (5). Fig. 1b represents only half of the yield surface (M < 0), while the other half (M > 0) is symmetric to the part shown.

$$j_{1,2} \circ N_k\left(a_k + \frac{N_k}{2 f_{cef} b_k}\right) + \left|M_k\right| \le 0 \tag{4}$$

$$j_{3,4} \circ mN_k + \left|V_k\right| \le 0 \tag{5}$$

2.2 Flow rule

Fig. 1a illustrates also the flow mode corresponding to crushing-hinging, in agreement with the normality rule. It is noted that, for the Coulomb criterion, the flow consists of a tangential displacement only. The flow rule at a joint can be written, in matrix form, as given by Eq. (6), and, in a component-wise form, as given by Eq. (7), in which the joint subscripts have been dropped for clarity. Here, $d\boldsymbol{\lambda}_k$ is the vector of the flow multipliers, with each flow multiplier corresponding to a yield surface, and satisfying Eqs. (8-9). These equations indicate that plastic flow must involve dissipation of energy, Eq. (8), and that plastic flow cannot occur unless the stresses have reached the yield surface, Eq. (9). For the entire structure, the flow rule results in Eq. (10), where the flow matrix $\mathbf{N_0}$ can be obtained by assembling all joint matrices.

$$d\mathbf{q}_k = \mathbf{N}_k d\boldsymbol{\lambda}_k \tag{6}$$

$$\begin{bmatrix} ds \\ dn \\ df \end{bmatrix} = \begin{bmatrix} 0 & 0 & -1 & 1 \\ a\left(1 - \frac{N}{f_{cef} b}\right) & a\left(1 - \frac{N}{f_{cef} b}\right) & 0 & 0 \\ -1 & 1 & 0 & 0 \end{bmatrix} \begin{bmatrix} dl_1 \\ dl_2 \\ dl_3 \\ dl_4 \end{bmatrix} \tag{7}$$

$$d\boldsymbol{\lambda}_k \ge \mathbf{0} \tag{8}$$

$$j_k^T d\boldsymbol{\lambda}_k = 0 \tag{9}$$

$$d\mathbf{q} = \mathbf{N}_0 d\boldsymbol{\lambda} \tag{10}$$

2.3 Compatibility

Compatibility between joint k generalized strains, and the displacement rates of the adjacent blocks i and j, is given in Eq. (11), being the vector $d\mathbf{u}_{i,j}$ defined in Eq. (12) and the matrix $\mathbf{C}_k$, given in Eq. (13). In this last equation a_k, β_i, β_j, are the angles, with respect to the x axis, of the direction of joint k, of the line defined by the centroid of block i and the centre of joint k, and of the line defined by the centroid of block j to the centre of joint k, respectively; and b_i, b_j, are the distances between the centre of joint k to the centroid of the blocks i and j, respectively.

$$d\mathbf{q}_k = \mathbf{C}_k d\mathbf{u}_{i,j} \tag{11}$$

$$d\mathbf{u}_{i,j} \circ \left\lfloor du_i \quad dv_i \quad dq_i \quad du_j \quad dv_j \quad dq_j \right\rfloor \tag{12}$$

$$\mathbf{C}_k = \left[\mathbf{C}_{ki} \quad \mathbf{C}_{kj}\right] = \left[\begin{array}{ccc|ccc} -\cos(a_k) & -\sin(a_k) & b_i \sin(b_i - a_k) & \cos(a_k) & \sin(a_k) & -b_j \sin(b_j - a_k) \\ \sin(a_k) & -\cos(a_k) & -b_i \cos(b_i - a_k) & -\sin(a_k) & \cos(a_k) & b_j \cos(b_j - a_k) \\ 0 & 0 & -1 & 0 & 0 & 1 \end{array}\right] \tag{13}$$

In order to extend the compatibility requirements to all the joints in the structure, supports must be included in the displacement rate vector. Supports are taken into account by adding fixed dummy blocks and, therefore, the displacement rates are split into block displacements, with subscript *B*, and support displacements, with subscript *S*. Similarly, the generalized strains are split into a basic set, with subscript *b*, and a redundant set, with subscript *r*. With this approach, the compatibility matrix is split into four sub-matrices, in such a way that Eq. (14) expresses the compatibility equations for the whole structure and the sub-matrix $\mathbf{C_{Bb}}$ is square and non-singular. Thus, after some manipulations, Eqs. (15) and (16) can be obtained.

$$\begin{bmatrix} d\mathbf{q_b} \\ d\mathbf{q_r} \end{bmatrix} = \begin{bmatrix} \mathbf{C_{Bb}} & \mathbf{C_{Sb}} \\ \mathbf{C_{Br}} & \mathbf{C_{Sr}} \end{bmatrix} \begin{bmatrix} d\mathbf{u_B} \\ d\mathbf{u_S} \end{bmatrix} \tag{14}$$

$$d\mathbf{u_B} = \mathbf{C_{Bb}^{-1}}\left[d\mathbf{q_b} - \mathbf{C_{Sb}}d\mathbf{u_S}\right] \tag{15}$$

$$d\mathbf{q_r} = \mathbf{C_{Br}}\mathbf{C_{Bb}^{-1}}\left[d\mathbf{q_b} - \mathbf{C_{Sb}}d\mathbf{u_S}\right] + \mathbf{C_{Sr}}d\mathbf{u_S} \tag{16}$$

The flow rule for the structure can be now re-written in the form of Eq. (17). Inserting this relation in Eq. (16), it is possible to obtain Eq. (18). This last equation represents the combination of compatibility and flow rule requirements, with the $d\mathbf{?}$ as unique variables. It is noted that, in the absence of movements at the supports, the right hand side of this equation vanishes. Furthermore, the inverse matrix $\mathbf{C_{Bb}}^{-1}$ can be easily calculated (or even, not explicitly calculated).

$$\begin{bmatrix} d\mathbf{q_b} \\ d\mathbf{q_r} \end{bmatrix} = \begin{bmatrix} \mathbf{N_{0b}} \\ \mathbf{N_{0r}} \end{bmatrix} d\mathbf{?} \tag{17}$$

$$\left(\mathbf{N_{0r}} - \mathbf{C_{Br}}\mathbf{C_{Bb}^{-1}}\mathbf{N_{0b}}\right)d\mathbf{?} = \left(\mathbf{C_{Sr}} - \mathbf{C_{Br}}\mathbf{C_{Bb}^{-1}}\mathbf{C_{Sb}}\right)d\mathbf{u_S} \tag{18}$$

2.4 Equilibrium

In a way similar to the used in the previous subsection, the generalized stresses are split into two sets, the basic one (subscript *b*) and the redundant one (subscript *r*). The external loads are also split into those applied to the blocks and those applied to the supports, i.e. reactions. Applying the contragradience principle, the equilibrium requirement is expressed by Eq. (19). From here, Eq. (20) follows directly, expressing the basic generalized stresses in terms of the redundant generalized stresses and the external loads. Once again, the matrix $\mathbf{C_{Bb}}^{-1}$ needs not to be calculated explicitly. Eq. (20) permits to consider solely the redundant stresses vector in the optimisation process, and to reduce the number of constraints. The second row of Eq. (19) can be used to obtain the reactions at the supports, once the solution is known.

$$\begin{bmatrix} \mathbf{F_{cB}} \\ \mathbf{F_{cS}} \end{bmatrix} + a\begin{bmatrix} \mathbf{F_{vB}} \\ \mathbf{F_{vS}} \end{bmatrix} = \begin{bmatrix} \mathbf{C_{Bb}^T} & \mathbf{C_{Br}^T} \\ \mathbf{C_{Sb}^T} & \mathbf{C_{Sr}^T} \end{bmatrix} \begin{bmatrix} \mathbf{Q_b} \\ \mathbf{Q_r} \end{bmatrix} \tag{19}$$

$$\mathbf{Q_b} = \mathbf{C_{Bb}^T}^{-1}\left[\mathbf{F_{cB}} + a\mathbf{F_{vB}} - \mathbf{C_{Br}^T}\mathbf{Q_r}\right] \tag{20}$$

2.5 Non-linear programming problem

The solution to a limit analysis problem must fulfil the previously discussed principles. In the presence of non-associated flow, there is no unique solution satisfying these principles and the actual failure load corresponds to the solution with a minimum load factor (Baggio and Trovalusci, 1998). The proposed mathematical description results in the non-linear programming problem expressed in Eqs. (21-27). Here, Eq. (21) is the objective function and Eq. (22) guarantees both compatibility and flow rule, being this last condition complemented with Eq. (27). Eq. (23) represents a scaling expression to the displacement rates (it can be replaced freely by other equations with a similar property) as, at the ultimate state, the displacement rates are undefined and it is only possible to determine their relative values. Equilibrium is given by Eq. (24), which does not add any constraint to the programming problem. Eq. (26) is the expression of the yield condition, which together with the flow rule must fulfil Eq. (25).

Minimize: a (21)

Subject to:

$$\left(\mathbf{N}_{0r} - \mathbf{C}_{Br}\mathbf{C}_{Bb}^{-1}\mathbf{N}_{0b}\right)d\mathbf{?} = \left(\mathbf{C}_{Sr} - \mathbf{C}_{Br}\mathbf{C}_{Bb}^{-1}\mathbf{C}_{Sb}\right)d\mathbf{u}_S \quad (22)$$

$$\mathbf{F}_{vB}^{T}d\mathbf{u}_B - 1 = 0 \quad (23)$$

$$\mathbf{Q}_b = \mathbf{C}_{Bb}^{T\ -1}\left[\mathbf{F}_{cB} + a\mathbf{F}_{vB} - \mathbf{C}_{Br}^{T}\mathbf{Q}_r\right] \quad (24)$$

$$j^{T}d\mathbf{?} = 0 \quad (25)$$

$$j \leq \mathbf{0} \quad (26)$$

$$d\mathbf{?} \geq \mathbf{0} \quad (27)$$

3 COMPUTER IMPLEMENTATION

The main objective of this research project is to develop an analysis tool suitable to be used in practical engineering projects, oriented to assess the seismic security of small and medium size ancient masonry buildings. For this reason, the computer implementation is done resorting to AutoCAD, in which the geometry of the block made structure is drawn. The developed application extracts the geometric data and pre-processes it. Complementary data is added as volumetric weights, block thickness, friction coefficient and compressive stress limit, in order to make the limit analysis in a FORTRAN written program. The same CAD package is used as post-processor to draw failure mechanisms and thrust lines (which generally have a meaning in the case of arches). During the development of this program, some noteworthy strategies needed to be implemented regarding the compatibility matrix and the solution procedure.

3.1 Compatibility matrix

Prior to the solution phase, it is necessary to build the compatibility matrix **C**. Due to the sparse nature of this matrix, an efficient storage strategy has been implemented. As the **C** matrix incorporates the joints matrices, $\mathbf{C}_{ki}$ and $\mathbf{C}_{kj}$, only the latter are stored, resorting to a given identifier integer number. Then, an *index* matrix, named $\mathbf{C}_{int}$, is built indicating the position of each joint matrix within the entire **C** matrix.

3.2 Optimisation

The non-linear mathematical problem given by Eqs. (21-27), is non-convex and complex to solve. The key issue is that non-linear programming algorithms require an initial estimate of the solution and, ideally, the first guess should be in the neighbourhood of the optimal solution and should be a feasible solution. Baggio and Trovalusci (1998) proposed to use the solution of the linearised problem, i.e. with associated flow rules, as initial guess to the problem with non-associated sliding flow rules. But, for the solution algorithm adopted in the present paper, this approach fails to converge. Gilbert (1998) used successive linear programming problems to approximate the solution of arches with limited compressive stresses. The strategies adopted here are (a) to use successive linear programming problems in order to approximate the solution to the non-linear programming problem with non-associated flow rules and limited compressive stresses; and (b) to solve the problem using a linearised solution with a smaller friction coefficient than μ; if convergence is not achieved with the original friction coefficient, successive attempts are made reducing each time this parameter in the initial linearised problem.

A successive quadratic programming routine is used to solve the general non-linear programming problem, see Visual Numerics (1997) for details. In particular, the gradients required by this routine are numerically calculated

It is important to stress that neither of the above strategies guarantees a solution with the absolute minimum load factor, being possible to obtain a local minimum instead. More research seems to be needed in solutions procedures able to capture the absolute minimum, but this is outside the scope of the present research project. From the engineering point of view, the solutions obtained

in the validation examples seem adequate regarding both the shape of the failure mechanism and the value of the limit load.

4 VALIDATION

For the purpose of validation of the model, a comparison was made between the results obtained with the developed program and experimental results of masonry structures available in the literature. Three rather different structural types have been selected. Traditionally, masonry arches have been adopted for validation of limit analysis methods whereas masonry shear walls have been adopted for validation of more sophisticated plane models. Here, firstly, the masonry arches tested by Royles and Hendry (1991) are considered; secondly, the unconfined shear walls tested by Oliveira (2000); and finally, the confined shear walls with opening tested by Vermeltfoort et al. (1993) and analysed with the finite element method by Lourenço (1996).

4.1 Masonry arches

Royles and Hendry (1991) performed a series of tests on scale models of masonry arch bridges. These models had geometric characteristics similar to those of three real bridges named Bridgemill, Bargower and Carron River. Here, only the tests of the arch-vaults with simulated fill dead load are modelled, because only on these circumstances it is possible to determine correctly the applied loads. The Bargower bridge results are not reported here because polystyrene blocks glued to the extrados of the experimental models modify its response in an unknown manner.

Table 1 shows the geometric characteristics of the tests models, and Table 2 provides the mechanical properties of the materials, as reported by Royles and Hendry (1991). The BM model had an additional load of 3 kN distributed uniformly over the upper surface. Loads distributed over the bridge width were applied at one fourth of the span. For analysis purposes, volumetric weights of 17 kN/m^3 and 22 kN/m^3 for the clay and concrete masonries were used, respectively. The masonry compressive strengths were estimated by the Mann's formula (Hendry 1998), see Eq. (28). Here, f_b is the brick strength, f_m is the mortar strength, and f_c is the masonry strength, all in N/mm^2. The effective compressive stresses used in the analyses were calculated by means of Eqs. (2-3). These are 4.48 N/mm^2 and 5.87 N/mm^2 for the clay bricks masonry and concrete bricks masonry, respectively.

Table 1: Geometric properties of the modelled bridges.

	Span	Rise	Width	Depth of the fill at crown	Vault thickness	Span/Rise
	mm	mm	mm	mm	mm	
Bridgemill	1000	158	466	12	38	6.4
Carron River	2480	750	570	52	103	3.4

Table 2: Material properties.

	Brick material	Brick strength N/mm^2	Mortar strength N/mm^2	Fill density kN/m^3
Bridgemill	Clay	19.5	1.47	14
Carron River	Concrete	30.0	1.47	14

$$f_c = 0.83 f_b^{0.66} f_m^{0.33} \tag{28}$$

The results in terms of failure loads are presented in the Table 3. The first two columns correspond to the experimental results, Royles and Hendry (1991), and the last column shows the results obtained by the present limit analysis model. For the Bridgemill model, it is observed that the numeric failure load agrees well with the experimentally measured values, which in turn are very similar between them. For the Carron River model, a large variation in the experimental failure load is observed. Nevertheless, the limit load calculated by the numeric model is close to the first test.

Table 3: Failure loads for the bridge models.

	Experiment 1 kN	Experiment 2 kN	Limit Analysis kN
Bridgemill	2.0	1.9	2.27
Carron River	2.6	4.0	2.40

4.2 Unconfined shear walls

Oliveira (2000) tested a series of shear walls under different levels of vertical load and monotonically increasing lateral load. The walls were made of stone blocks laid without mortar between them, see Fig. 2a. The wall thickness was 200 mm. The mean compressive strength, measured on prisms of three and four dry laid stone blocks, was 57.1 N/mm^2. The corresponding effective compressive stress calculated according to Eqs. (2-3) is 23.7 N/mm^2. Series of two specimens with vertical loads of 30kN, 100kN and 200kN were performed, named SW30, SW100 and SW200, respectively.

As part of the present project, finite element micro-models of these walls were made using the interface element model proposed by Lourenço (1996). Non-linear analyses for the SW30 and SW200 specimens were performed. Limit analyses were performed for the SW30, SW100 and SW200 walls. Figs. 2b-2d present the horizontal load-displacement curves for the top beam for the three walls studied. In these figures, the experimentally obtained results are compared with those of the FEM analyses, and with the limit loads calculated using the approach presented in this paper.

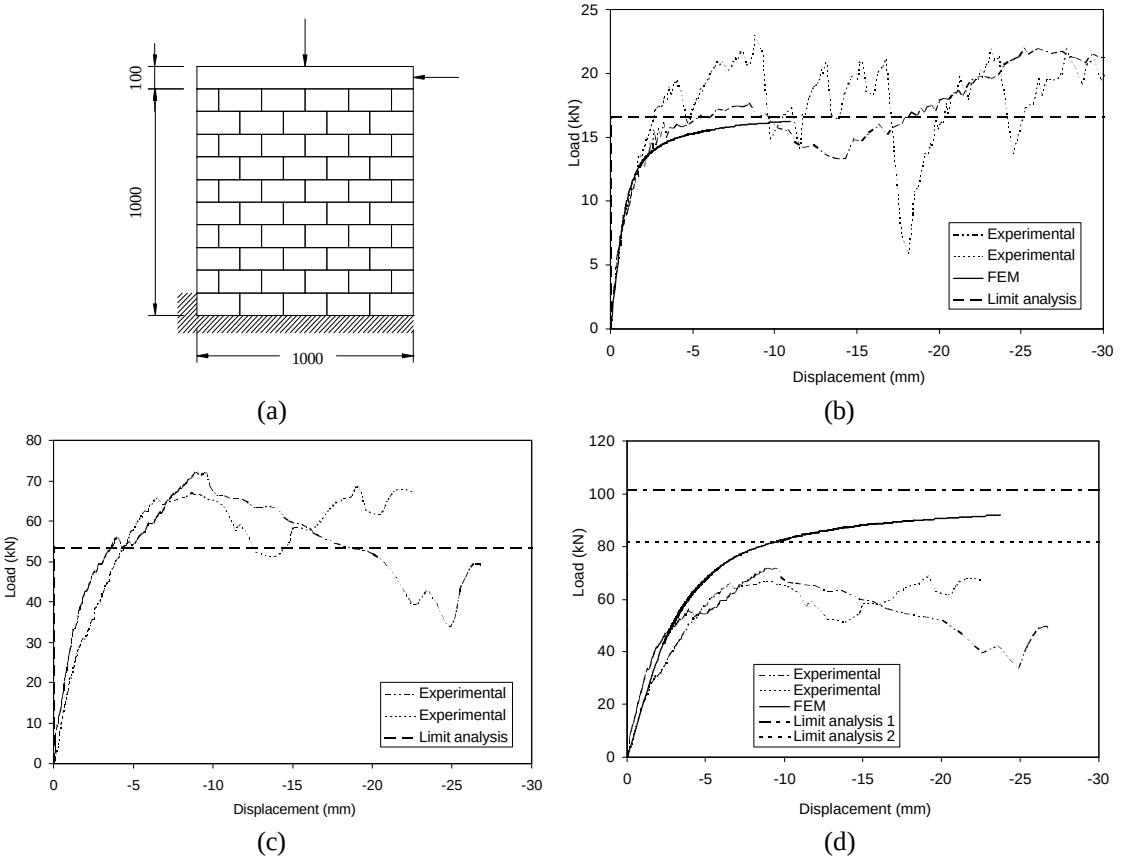

Figure 2: Shear walls; (a) general arrangement; (b) SW30 load-displacement curves; (c) SW100 load-displacement curves; (d) SW200 load displacement curves.

For the SW30 wall, a good agreement between the experimental and the FEM analysis results is observed. Also, it can be observed that the limit analysis result gives a good approximation to the failure load, in fact, as it should be expected, the FEM curve seems to asymptotically con-

verge for this load. The failure mechanisms are very similar for the experiments and the two numerical models (FEM and limit analysis), namely, a stepwise separation of blocks along the compression diagonal with the upper part rotating over the wall base, and practically without stone crushing or cracking, see Fig. 3a.

In the case of the SW100 wall, the limit analysis calculated load also agrees well with the experimental results. The failure mechanisms observed in the experiments and in the limit analysis calculation are similar to the one described for SW30 walls, but limited stone crushing and stone cracking was also observed in the tests.

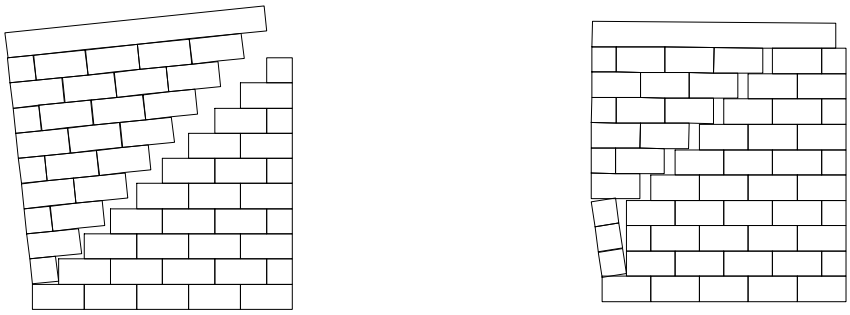

(a) (b)

Figure 3: Failure modes for SW200 model; (a) without block cracking; (b) with cracking of one block.

The SW200 experimental models exhibited a different failure mechanism, with severe stone crushing and stone cracking along the compressed diagonal, together with slipping over the horizontal joints. In the finite element model stone cracking was not included and this is presumably the cause for the higher load obtained at large displacement levels, with respect to the experimental values. The limit analysis program, where each masonry block was modelled as a rigid block (limit analysis 1, in Fig. 2d), also gives a very large load compared with the experimental models failure loads. Again, some asymptotic convergence of the FEM load-displacement diagram to the limit analysis solution seems to be found. The failure mechanism obtained continues to be the same of the previous models, see Fig. 3a.

A second analysis (limit analysis 2 in Fig. 2d) was performed in order to assess the effect of considering cracking of the leftmost block in the third course, see Fig. 3b; this hypothesis arises from the observation of the experimental failure modes. The new obtained failure mechanism is more in agreement with the experimental observations, and the limit load gives a better approximation to those experimentally obtained. It is interesting to observe how an apparently small modification in the model suffices to completely modify both the failure mechanism and the limit load.

4.3 Confined shear walls

Vermeltfoort et al. (1993) tested a series of shear walls with an opening, illustrated in Fig. 4a. The upper edge of these walls was restrained to move in the vertical direction and to rotate. A vertical pre-compression load of 30 kN was applied prior to the horizontal force. The experimental compressive strength used by Lourenço (1996) was 10.5 N/mm^2, to which corresponds an effective stress of 6.8 N/mm^2, according to Eqs. (2-3). The walls thickness was 100 mm.

This problem has two special aspects to be considered from a limit analysis perspective. Firstly, to maintain the wall confined, the sum of the elastic and plastic vertical deformations must be zero, and, in a limit analysis solution, the elastic deformations are unknown. The second aspect concerns the solution procedure, as with the herein proposed approach a straightforward solution for this problem cannot be obtained, namely, if the upper beam restriction is introduced in the model, the initial linear problem has no solution. This problem arises either if the dilatancy coefficient is not equal to zero or if hinging failure modes occur. Therefore, the analysis must be tackled in an indirect form, assuming that the upper beam is not restrained and a load is applied on it. The vertical load, V, and its distance from the wall edge, d, are sought by an iterative procedure, in such a way that the rotation and vertical displacement rates of the top beam yield the prescribed values.

In view of such iterative procedure and in order to illustrate how the present approach is intended to be used in practical applications, a simplified model of the wall was proposed, see Fig. 4b. The topology of this model is inspired by the failure mechanisms observed both, experimentally (Vermeltfoort et al. 1993) and numerically (Lourenço 1996).

A first limit analysis (Analysis 1) was made without taking into account the elastic deformations, see Table 4 and Fig. 4c. It is observed that both, the vertical and horizontal loads at collapse are around twice the experimental values. Fig. 4c presents also clearly visible crushed zones, i.e. the apparent overlapping between blocks. A second limit analysis (Analysis 2) was performed with the mean experimental vertical load value, applied at the location *d* needed to prevent rotation of the upper beam, see Table 4 and Fig. 4d. In this case the limit load agrees much better with the experimental value, although, the distances from the edge to the load differ considerably. In Fig. 4d a displacement upwards is observed as expected, being the ratio between vertical and horizontal displacement rates 0.324. The peak load is obtained at about 5 mm of horizontal displacement (Lourenço 1996), which means that a 1.6 mm vertical elastic displacement would be needed to maintain the wall perfectly confined. With the 8000 N/mm^2 measured Young modulus (Vermeltfoort et al. 1993), and the vertical load applied, a vertical elastic displacement of about 0.13 mm can be calculated. Thus, the initial tangential vertical stiffness is about twelve times the peak secant stiffness, which seems reasonable.

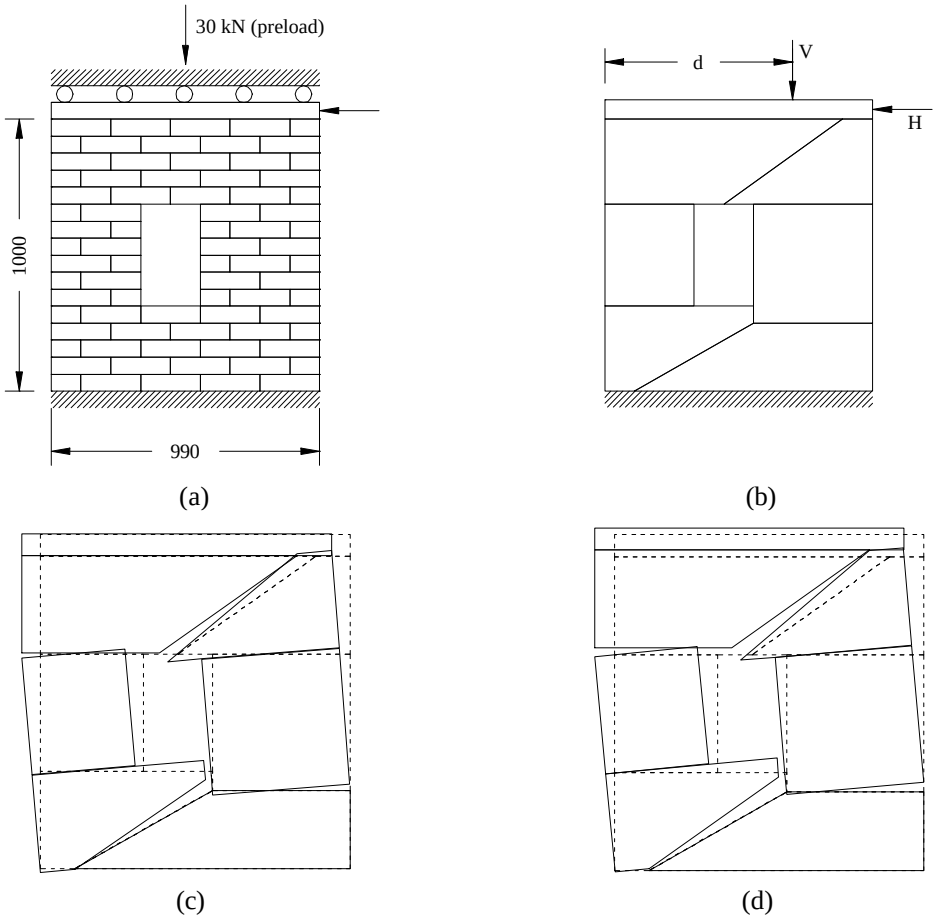

Figure 4: Confined shear wall; (a) general arrangement; (b) simplified model; (c) Analysis 1 failure mechanism; (d) Analysis 2 failure mechanism.

Table 4: Confined shear wall results

	H kN	*V* kN	*d* m
Experimental[a]	40.4	102.1	0.540
Analysis 1	71.7	236.0	0.673
Analysis 2	45.1	102.1	0.779

[a] Average of three tests.

5 CONCLUSIONS

The limit analysis approach presented in this paper has the potential to become a powerful tool for the small and medium size ancient masonry structures assessment in the engineering practice. In particular, the approach avoids, on one hand, the use of sophisticated and time consuming non-linear FE techniques, and, on the other hand, oversimplified assumptions. The formulation presented also offers a more general treatment of yield and flow functions, with respect to previous proposals, e.g. Baggio and Trovalusci (1998) and Gilbert (1998).

Its validation through three structures with very different behaviour, has demonstrated that good agreement with failure loads and failure mechanisms can be obtained. These examples also have shown that the results are very sensible to the model topology, and additional effort is needed in order to provide recommendations on how to divide a structure in rigid blocks, so that a good approximation of the critical failure mechanism can be obtained in a reasonable computing time.

An open issue is the adequate value of the effective compressive stress. In this paper, the adopted values, which resulted from reinforced concrete investigations, seem to have given good results in the validation examples presented. However, the rather large scatter in the experimental results can mask this apparent agreement. In the case of arches and unconfined masonry structures, it is known that the failure is related, generally, to instability effects, triggered by the no tension strength, rather than to exhausting the material compressive capacity. The case of the confined masonry walls, where failure is usually accompanied by material crushing, seems of less interest for historical masonry structures in its original state, as they are hardly confined.

ACKNOWLEDGMENTS

The first author wishes to thank the scholarships made available to pursue his PhD studies by the Consejo Nacional de Ciencia y Tecnología and the Secretaría de Educación Pública of Mexico. The work was also partially supported by project SAPIENS 33935-99 funded by Fundação para a Ciência e Tecnologia of Portugal.

REFERENCES

Baggio, C. and Trovalusci, P. 1998. Limit analysis for no-tension and frictional three-dimensional discrete systems. *Mechanics of Structures and Machines,* 26(3), p. 287-304.

Begg, D.W. and Fishwick, R.J. 1995. Numerical analysis of rigid block structures including sliding. *Proc. 3rd Int. Symp. Comp. Meth. Struct. Mas.*, Portugal, eds. J. Middleton, G.N. Pande.

Gilbert, M. and Melbourne, C. 1994. Rigid-block analysis of masonry structures. *The Struct. Engineer,* 72(21), p. 356-361.

Gilbert, M. 1998. On the analysis of multi-ring brickwork bridges. In A. Sinopoli (ed) *Arch Bridges*, p. 109-118. Rotterdam: Balkema.

Hendry, A. W. 1998. *Structural Masonry, second edition*. London: Macmillan Press LTD.

Heyman, J. 1969. The safety of masonry arches. *Int. J. Mech. Sci.*, vol. 11, p. 363-385.

Livesley, R.K. 1978, Limit analysis of structures formed from rigid blocks. *Int. J. Num. Meth. Engrg.*, 12, p. 1853-1871.

Lourenço, P.B. and Rots, J.G. 1997. A multi-surface interface model for the analysis of masonry structures. *J. Engrg. Mech., ASCE,* 123(7), p. 660-668.

Lourenço, P.B., Rots, J.G. and Blaauwendraad, J. 1998. Continuum model for masonry: Parameter estimation and validation. *J. Struct. Engrg., ASCE*, 124(6), p. 642-652.

Lourenço, P.B. 1996. Computational strategies for masonry structures. PhD Thesis. Delft University of Technology. Delft, Netherlands.

Oliveira, D.V. 2000. Mechanical characterization of stone and brick masonry. Report 00-DEC/E-4, Universidade do Minho. Guimarães, Portugal.

Royles, R. and Hendry, A. W. 1991. Model tests on masonry arches. *Proc. Instn. Civ. Engrs, part 2*, 91, June, p. 299-321.

Vermeltfoort, A. T., Raijmakers, T. M. J., and Jansen, H. J. M. 1993. Shear tests on masonry walls. *6th North American Masonry Conference*, June 6-9, Philadelphia, USA.

Visual Numerics. 1997. *IMSL MATH/Library User's Manual*. Boulder: Visual Numerics, Inc.